Accelerator-System Solutions for Broad-Beam Ion Sources

Harold R. Kaufman*
Colorado State University, Fort Collins, Colo.

Over 300 space-charge-flow solutions were obtained on a digital computer for an electron-bombardment ion source. Results are presented in both tabular and generalized graphical form for a wide range of geometries and operating conditions.

Introduction

SPACE-charge-flow solutions are useful for both the design of accelerator systems and the interpretation of experimental performance from such systems. A recent survey of electron-bombardment thruster technology included only 28 axisymmetric space-charge-flow solutions in which both acceleration and deceleration regions were simulated for multiaperture configurations.[1] These solutions had been obtained by Lathem[2,3] and Nudd and Amboss.[4] The present study includes over 300 additional solutions, thereby substantially increasing the number of published solutions. The digital computer program of Bogart and Richley[5] was used in the present study, together with the plasma sheath condition of Hyman et al.[6] and the closure surface technique of Pawlik et al.[7] The use of one computer program and one iteration procedure hopefully avoids some of the scatter that would otherwise be introduced. Although some advantages have been shown for conical hole shapes,[1] only cylindrical holes were used herein because of their ease of fabrication and widespread use.

Method of Solution

A screen-hole radius corresponding to 10 mesh squares was used throughout. A larger number of squares would have given greater accuracy, but the required computer time increases at least as the second power of the number of squares in a radius for otherwise similar configurations. Inasmuch as well over 100 hr of computer time were used in this study, any substantial increase in the time per solution would have resulted in a reduction in the number of solutions investigated.

The upstream plasma sheath was assumed to consist of 10 straight-line segments, with the segments corresponding in location to the 10 mesh squares of radius. This sheath position was iterated to give an ion-current density uniform to better than ±5%. For the closure surface of the deceleration region, a simple plane surface was used.† This plane was oriented normal to the mean ion-beam direction. The ions have high velocities in the vicinity of the closure surface and are therefore only slightly perturbed by the approximation of the actual complex shape by a plane surface. The procedure for locating the closure surface used the radius from the axis of the beam (from a single hole) within which half the ion-beam current passed. The axial location of the plane closure surface was then selected to give zero electric field at this radius. Most solutions were iterated to find this axial location within one mesh square. The fraction of open screen area was not found to be a significant parameter in previous studies,[1,2] so this parameter was not varied. The outer radius of the axisymmetric region was assumed to be 15 mesh squares from the axis, which corresponded to 44% open screen area.

The high degree of mathematical accuracy that can be obtained with digital computers often gives an unwarranted impression of an accurate simulation of nature. The finite size of the mesh squares, together with the program assumptions necessary for the use of a finite mesh, can result in substantial data scatter. In an extreme case, a movement of the upstream plasma sheath (at a point intermediate of the axis and outer edge) of 0.01 mesh squares resulted in changes of 20% in total beam current and 30% in maximum half-angle – while maintaining current-density uniformity to better than ±5%. Inasmuch as a change of this small size should have resulted in trivial changes in currents and angles, the solutions presented herein must be considered to have an uncertainty of at least ±10% in current and ±15% in angle. Some attempt to reduce scatter was made in that solutions were omitted when they were found to depart sharply from general trends. There is, however, no assurance that systematic errors of the magnitudes given are not present in the data presented herein.

Accelerator-System Parameters

The definitions of the various accelerator-system measurements are given in Fig. 1. The decelerator grid is omitted in two-grid systems, but when it is present it has the same thickness and upstream spacing as the accelerator grid. (That is, $t_a = t_d$ and ℓ_g is the same for both interelectrode gaps.) The total acceleration voltage (potential difference) and the net acceleration voltage are both indicated in Fig. 2. The net-to-total voltage ratio R is the ratio of these two voltages, as is also indicated in Fig. 2. When a decelerator grid is used, it is assumed to be at ground potential (the potential of the ion beam).

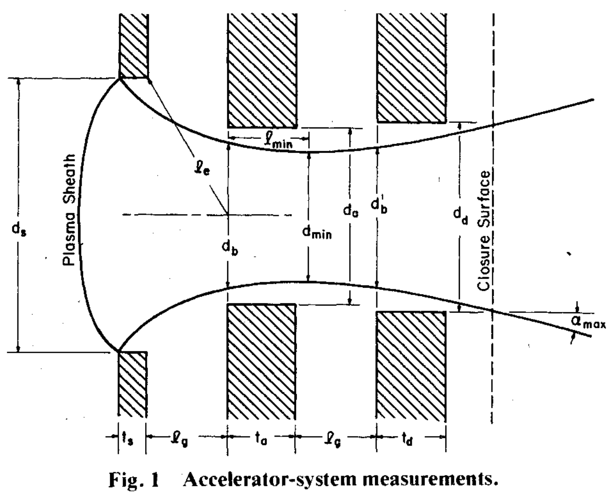

Fig. 1 Accelerator-system measurements.

Presented as Paper 75-430 at the AIAA 11th Electric Propulsion Conference, New Orleans, La., March 19-21, 1975; submitted Jan. 18, 1977; revision received April 1, 1977.

Index categories: Aerospace Technology Utilization; Analytical and Numerical Methods; Electric and Advanced Space Propulsion.

*Professor. Associate Fellow AIAA.

†A flat plane closure surface is a reasonable assumption only for a multiaperture accelerator system.

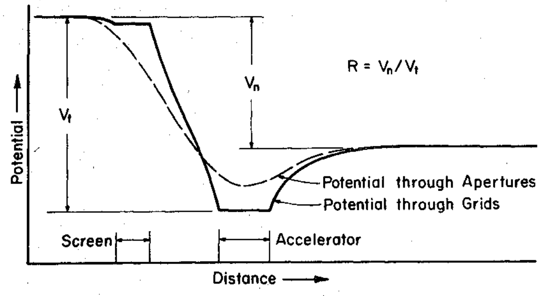

Fig. 2 Variation of potential through 2-grid accelerator system.

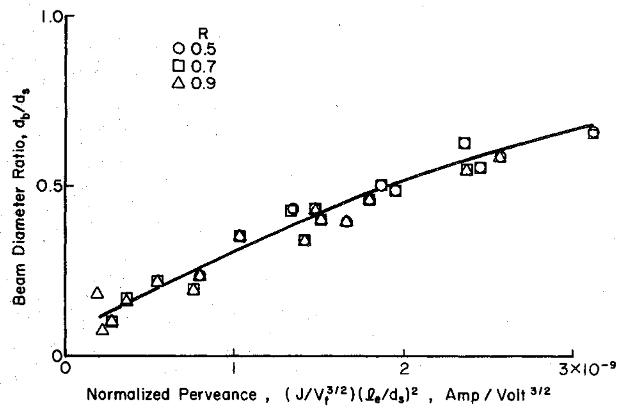

Fig. 3 Ion beam diameter at entrance to accelerator hole. ℓ_g/d_s = 0.2-0.7.

The solutions presented in graphical form herein are given in terms of a "normalized perveance," which is defined as $(J/V_t^{3/2})(\ell_e/d_s)^2$. With singly ionized mercury, a value of 3.03×10^{-9} A/V$^{3/2}$ corresponds to Child's law current density over the area of the screen hole. With lighter propellants, the Child's law value would be increased by the square root of the ion-mass ratio. Some solutions were attempted with plasma sheaths moved further downstream in an attempt to obtain a normalized perveance well above the 3.03×10^{-9} value. These solutions were hard to converge for uniform current-density at the sheath, had highly divergent ion beams, and did not end up significantly above the 3.03×10^{-9} value.

This normalized perveance was introduced to offset most of the effects of different interelectrode gaps, or spacings.[1] That is, accelerator-system solutions are correlated better by the use of this perveance than any present alternative. The use of the current J through a single hole is conventional, as well as the use of the total acceleration voltage. The use of some acceleration distance in a ratio with the screen-hold diameter d_s is also conventional. The unusual aspect of normalized perveance is the use of the measurement ℓ_e as the effective acceleration length. Although the best justification of the use of the ℓ_e is in the degree of correlation obtained, a qualitative justification of the use of this acceleration length can also be given. At very small values of ℓ_g/d_s, the acceleration is substantially spherical and the acceleration length is approximately $d_s/2$. With very large values of ℓ_g/d_s, the acceleration approaches the planar case with an acceleration length of approximately ℓ_g. The use of the diagonal distance ℓ_e, which in mathematical form is

$$\ell_e = (\ell_g^2 + d_s^2/4)^{1/2}$$

results in a gradual transition between these two extremes.

Two-Grid Solutions

The solutions obtained using only a screen grid and an accelerator grid are presented in Table 1 and Figs. 3-7. It was found that the best focusing is generally obtained by using an accelerator hole that is only slightly larger than the beam passing through it. The majority of the two-grid survey was therefore made using accelerator holes that were larger than the largest diameter of the beams passing through them by about 10% of the screen hole diameter. This latter amount (corresponding to one mesh square in radius) was felt to approximate the minimum experimental tolerance that could be achieved. Because of their greater interest, only these small accelerator-hole data are included in Figs. 3-5 and 7. The data of Figs. 3 and 4 are further restricted by omitting data with the largest value of ℓ_g/d_s (1.0). This latter restriction should not be serious inasmuch as most present designs utilize much lower values of ℓ_g/d_s. For those few applications that require a large value of ℓ_g/d_s, the solutions can be found in Table 1. Most of the solutions obtained were for an accelerator thickness equal to 0.25 of the screen hole diameter.

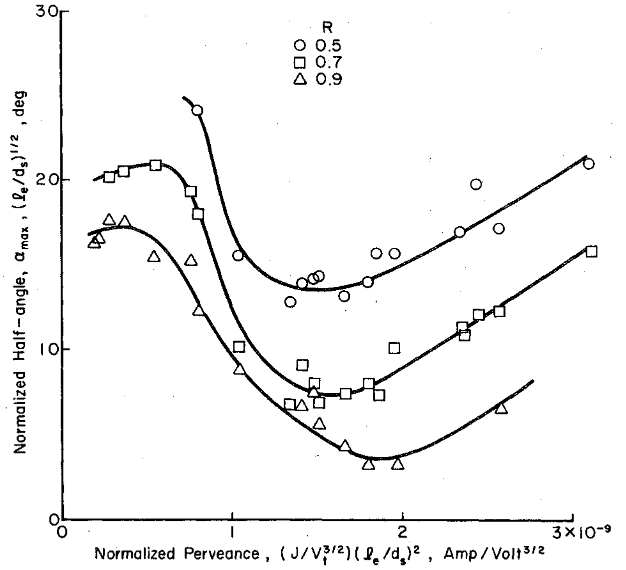

Fig. 4 Normalized beam spread for 2-grid configurations. ℓ_g/d_s = 0.2-0.7.

The diameter of the ion beam at the entrance (upstream end) of the accelerator hole is shown in Fig. 3. The effects of R and ℓ_g/d_s are both seen to be small over the ranges covered, in that essentially one curve is obtained for all solutions. Most operating conditions of interest (except perhaps the highest perveances) correspond to a beam diameter that becomes smaller after it enters the accelerator hole. Thus Fig. 3 will usually be sufficient to size the accelerator hole.

The maximum half-angle α_{max} of the ion beam (downstream of the closure plane) is shown in Fig. 4 for $R=0.7$. The product ℓ_{max} (ℓ_e/d_s) served to correlate the limited number of solutions available for an earlier study,[1]‡ but α_{max} $(\ell_e/d_s)^{1/2}$ was found to give a better correlation of the solutions presented herein. The maximum half-angle is plotted in normalized form, α_{max} $(\ell_e/d_s)^{1/2}$ in Fig. 4 for values of ℓ_g/d_s from 0.2 to 0.7 and values of R from 0.5 to 0.9. The solutions are, within the scatter, generalized to one curve for each value of R.

The screen thickness corresponding to the various operating conditions are given in Fig. 5. The screen thickness was determined by the axial location of the sheath at the point where it intercepted the side of the screen hole. Note that the value of R does not significantly affect the sheath location, so that Fig. 5 applies to all R values. Also note that this iterated value of screen thickness was not given in the earlier study.[1]

‡The factor $R^{1/2}$ was also included in the correlating parameter of the elarlier study, but the inclusion of this factor only correlated solutions for various R values over part of the perveance range covered.

Table 1 Two-grid solutions

t_s/d_s	ℓ_g/d_s	t_a/d_s	d_a/d_s	R	$J/V_t^{3/2}$ (nano-pervs/hole)	d_b/d_s	d_{min}/d_s	ℓ_{min}/d_s	α_{max} (deg)	C_f	R_{max}
0.34	0.20	0.25	0.27	0.95	1.28	0.16	0.07	0.30	21.5	0.979	0.958
0.34	0.30	0.25	0.21	0.95	0.83	0.10	0.06	0.16	21.7	0.973	0.965
0.26	0.30	0.25	0.33	0.95	1.62	0.22	0.10	0.47	15.8	0.989	0.950
0.34	0.50	0.25	0.32	0.95	0.43	0.07	0.05	-0.04	19.0	0.977	>0.975
0.18	0.50	0.25	0.34	0.95	1.60	0.23	0.12	0.74	12.3	0.9950	0.962
0.34	0.70	0.25	0.42	0.95	0.27	0.18	0.04	-0.25	17.1	0.982	>0.975
0.16	0.70	0.25	0.30	0.95	1.03	0.20	0.14	0.37	14.6	0.9908	0.966
0.09	0.70	0.25	0.44	0.95	1.91	0.34	0.29	>1.00	7.5	0.9985	0.957
0.09	0.70	0.25	0.50	0.95	2.24	0.40	0.38	0.40	5.0	0.9995	0.956
0.34	1.00	0.25	0.55	0.95	0.16	0.32	0.04	-0.55	15.1	0.985	>0.975
0.18	1.00	0.25	0.24	0.95	0.59	0.10	0.09	0.12	14.3	0.9931	>0.975
0.09	1.00	0.25	0.38	0.95	1.12	0.27	0.25	0.42	7.1	0.9987	0.974
0.06	1.00	0.25	0.62	0.95	1.86	0.51	0.51	0.01	4.1	0.9988	0.957
0.34	0.20	0.25	0.27	0.90	1.28	0.16	0.07	0.30	24.0	0.969	---
0.34	0.30	0.25	0.21	0.90	0.83	0.10	0.06	0.16	23.0	0.968	---
0.26	0.30	0.25	0.33	0.90	1.62	0.22	0.10	0.46	20.2	0.988	---
0.18	0.30	0.25	0.46	0.90	3.05	0.35	0.24	0.50	11.5	0.9967	0.923
0.34	0.50	0.25	0.32	0.90	0.43	0.07	0.05	-0.05	19.6	0.976	---
0.18	0.50	0.25	0.34	0.90	1.60	0.23	0.14	0.53	14.6	0.9954	---
0.10	0.50	0.25	0.50	0.90	3.02	0.40	0.36	0.42	6.7	0.9987	0.929
0.09	0.50	0.25	0.56	0.90	3.60	0.46	0.43	0.24	3.8	0.9992	0.918
0.34	0.70	0.25	0.42	0.90	0.27	0.18	0.04	-0.25	17.6	0.980	---
0.16	0.70	0.25	0.30	0.90	1.03	0.20	0.14	0.37	16.4	0.989	---
0.09	0.70	0.25	0.44	0.90	1.91	0.34	0.31	0.47	7.2	0.9987	---
0.09	0.70	0.25	0.50	0.90	2.24	0.40	0.38	0.34	4.6	0.9994	---
0.06	0.70	0.25	0.66	0.90	3.20	0.55	0.55	0.03	6.6	0.9964	0.926
0.34	1.00	0.25	0.55	0.90	0.16	0.32	0.04	-0.55	15.6	0.985	---
0.18	1.00	0.25	0.24	0.90	0.59	0.10	0.09	0.12	15.2	0.9914	---
0.09	1.00	0.25	0.38	0.90	1.12	0.27	0.25	0.35	7.5	0.9986	---
0.09	1.00	0.25	0.43	0.90	1.31	0.33	0.32	0.38	5.1	0.9994	>0.950
0.06	1.00	0.25	0.62	0.90	1.86	0.51	0.51	0.01	5.0	0.9981	---
0.34	0.20	0.25	0.27	0.85	1.28	0.16	0.07	0.30	25.2	0.965	---
0.19	0.20	0.25	0.54	0.85	4.62	0.43	0.33	0.37	9.4	0.9978	0.888
0.13	0.20	0.25	0.60	0.85	6.41	0.50	0.44	0.28	8.5	0.9976	0.856
0.34	0.30	0.25	0.21	0.85	0.83	0.10	0.06	0.16	23.7	0.966	---
0.26	0.30	0.25	0.33	0.85	1.62	0.22	0.10	0.47	23.1	0.980	---
0.18	0.30	0.25	0.46	0.85	3.05	0.35	0.24	0.48	11.5	0.9969	---
0.13	0.30	0.25	0.53	0.85	4.36	0.43	0.36	0.30	9.6	0.9976	0.897
0.10	0.30	0.25	0.59	0.85	5.74	0.49	0.46	0.24	5.6	0.9976	0.878
0.34	0.50	0.25	0.32	0.85	0.43	0.73	0.05	-0.04	20.3	0.974	---
0.18	0.50	0.25	0.34	0.85	1.60	0.23	0.14	0.52	13.7	0.9956	---
0.09	0.50	0.25	0.56	0.85	3.60	0.46	0.43	0.23	4.8	0.9983	---
0.06	0.50	0.25	0.70	0.85	5.16	0.59	0.58	0.05	9.6	0.9920	0.897
0.34	0.70	0.25	0.42	0.85	0.27	0.18	0.04	-0.25	18.2	0.979	---
0.16	0.70	0.25	0.30	0.85	1.03	0.20	0.14	0.37	17.6	0.987	---
0.09	0.70	0.25	0.44	0.85	1.91	0.34	0.31	0.49	7.0	0.9985	---
0.09	0.70	0.25	0.50	0.85	2.24	0.40	0.38	0.33	4.3	0.9990	---
0.06	0.70	0.25	0.66	0.85	3.20	0.55	0.55	0.03	7.8	0.9949	---
0.34	1.00	0.25	0.55	0.85	0.16	0.32	0.04	-0.55	16.1	0.984	---
0.18	1.00	0.25	0.24	0.85	0.59	0.10	0.09	0.12	16.1	0.989	---
0.09	1.00	0.25	0.38	0.85	1.12	0.27	0.25	0.38	8.6	0.9979	---
0.09	1.00	0.25	0.43	0.85	1.31	0.33	0.32	0.36	5.0	0.9989	---
0.06	1.00	0.25	0.62	0.85	1.86	0.51	0.51	0.01	6.2	0.9972	---
0.34	0.20	0.25	0.27	0.80	1.28	0.16	0.07	0.30	26.4	0.960	---
0.19	0.20	0.25	0.54	0.80	4.61	0.43	0.34	0.34	9.5	0.9979	---
0.13	0.20	0.25	0.60	0.80	6.40	0.50	0.44	0.27	8.0	0.989	---
0.10	0.20	0.25	0.65	0.80	8.45	0.56	0.52	0.16	11.1	0.9920	0.832
0.34	0.30	0.25	0.21	0.80	0.83	0.10	0.06	0.16	24.6	0.963	---
0.26	0.30	0.25	0.33	0.80	1.62	0.22	0.10	0.47	25.1	0.974	---
0.18	0.30	0.25	0.46	0.80	3.05	0.35	0.24	0.48	11.4	0.9967	---
0.13	0.30	0.25	0.53	0.80	4.36	0.42	0.36	0.30	9.1	0.9967	---
0.10	0.30	0.25	0.59	0.80	5.74	0.49	0.46	0.24	8.9	0.9945	---
0.08	0.30	0.25	0.73	0.80	6.91	0.63	0.56	0.25	10.0	0.9910	0.841
0.06	0.30	0.25	0.80	0.80	9.19	0.66	0.66	0.02	16.4	0.976	0.818
0.34	0.50	0.25	0.32	0.80	0.43	0.07	0.05	-0.05	20.9	0.972	---
0.18	0.50	0.25	0.34	0.80	1.60	0.23	0.14	0.53	17.2	0.9936	---
0.10	0.50	0.25	0.50	0.80	3.02	0.40	0.36	0.37	5.9	0.9978	---
0.09	0.50	0.25	0.56	0.80	3.60	0.46	0.43	0.23	6.1	0.9973	---
0.06	0.50	0.25	0.70	0.80	5.15	0.59	0.58	0.05	13.1	0.987	---
0.34	0.70	0.25	0.42	0.80	0.27	0.18	0.04	-0.25	18.7	0.978	---

Table 1 continued

t_s/d_s	ℓ_g/d_s	t_a/d_s	d_a/d_s	R	$J/V_t^{3/2}$ (nano-pervs/hole)	d_b/d_s	d_{min}/d_s	ℓ_{min}/d_s	α_{max} (deg)	C_f	R_{max}
0.16	0.70	0.25	0.30	0.80	1.03	0.20	0.14	0.37	18.8	0.983	---
0.09	0.70	0.25	0.44	0.80	1.91	0.34	0.31	0.47	7.2	0.9976	---
0.09	0.70	0.25	0.50	0.80	2.24	0.40	0.38	0.33	4.5	0.9984	---
0.06	0.70	0.25	0.66	0.80	3.20	0.55	0.55	0.03	9.2	0.9930	---
0.34	1.00	0.25	0.55	0.80	0.16	0.32	0.04	-0.55	16.6	0.982	---
0.18	1.00	0.25	0.24	0.80	0.59	0.10	0.09	0.12	16.8	0.987	---
0.09	1.00	0.25	0.38	0.80	1.12	0.27	0.25	0.36	9.7	0.9968	---
0.09	1.00	0.25	0.43	0.80	1.31	0.33	0.32	0.36	5.0	0.9983	---
0.06	1.00	0.25	0.62	0.80	1.86	0.51	0.51	0.01	7.3	0.9960	---
0.34	0.20	0.25	0.27	0.70	1.26	0.16	0.07	0.32	28.0	0.955	---
0.19	0.20	0.25	0.54	0.70	4.61	0.43	0.34	0.33	9.2	0.9957	---
0.13	0.20	0.25	0.60	0.70	6.40	0.50	0.44	0.26	10.1	0.9917	---
0.10	0.20	0.25	0.65	0.70	8.44	0.56	0.52	0.16	16.6	0.983	---
0.34	0.30	0.25	0.21	0.70	0.83	0.11	0.06	0.16	26.4	0.957	---
0.26	0.30	0.25	0.33	0.70	1.62	0.22	0.10	0.47	27.4	0.964	---
0.18	0.30	0.25	0.46	0.70	3.05	0.35	0.25	0.48	13.4	0.9922	---
0.13	0.30	0.25	0.53	0.70	4.36	0.43	0.36	0.29	10.5	0.9925	---
0.10	0.30	0.25	0.59	0.70	5.74	0.49	0.46	0.23	13.4	0.988	---
0.08	0.30	0.25	0.73	0.70	6.90	0.63	0.57	0.25	14.9	0.983	---
0.06	0.30	0.25	0.80	0.70	9.17	0.66	0.65	0.08	20.9	0.962	---
0.18	0.50	0.25	0.34	0.70	1.60	0.23	0.14	0.53	21.4	0.987	---
0.10	0.50	0.25	0.50	0.70	3.02	0.40	0.36	0.36	8.2	0.9941	---
0.09	0.50	0.25	0.56	0.70	3.60	0.46	0.43	0.22	9.5	0.9934	---
0.06	0.50	0.25	0.70	0.70	5.15	0.59	0.58	0.05	14.7	0.983	---
0.16	0.70	0.25	0.30	0.70	1.03	0.20	0.14	0.37	20.8	0.978	---
0.09	0.70	0.25	0.44	0.70	1.91	0.34	0.31	0.46	9.8	0.9930	---
0.09	0.70	0.25	0.50	0.70	2.24	0.40	0.38	0.32	8.0	0.9952	---
0.06	0.70	0.25	0.66	0.70	3.20	0.55	0.55	0.03	11.9	0.989	---
0.18	1.00	0.25	0.24	0.70	0.59	0.10	0.09	0.12	18.2	0.984	---
0.09	1.00	0.25	0.38	0.70	1.12	0.27	0.25	0.38	12.9	0.9929	---
0.09	1.00	0.25	0.43	0.70	1.31	0.33	0.32	0.35	7.3	0.9956	---
0.06	1.00	0.25	0.62	0.70	1.86	0.51	0.51	0.01	9.5	0.9935	---
0.19	0.20	0.25	0.54	0.60	4.61	0.43	0.34	0.32	12.2	0.989	---
0.13	0.20	0.25	0.60	0.60	6.40	0.50	0.44	0.25	15.5	0.982	---
0.10	0.20	0.25	0.65	0.60	8.44	0.56	0.52	0.16	21.6	0.970	---
0.26	0.30	0.25	0.33	0.60	1.62	0.22	0.10	0.47	29.9	0.955	---
0.18	0.30	0.25	0.46	0.60	3.05	0.35	0.25	0.48	16.7	0.978	---
0.13	0.30	0.25	0.53	0.60	4.36	0.43	0.36	0.27	14.2	0.986	---
0.10	0.30	0.25	0.59	0.60	5.73	0.49	0.46	0.23	17.0	0.981	---
0.08	0.30	0.25	0.73	0.60	6.89	0.63	0.57	0.25	18.1	0.973	---
0.06	0.30	0.25	0.80	0.60	9.15	0.66	0.66	0.02	24.3	0.950	---
0.18	0.50	0.25	0.34	0.60	1.60	0.23	0.14	0.53	25.1	0.979	---
0.10	0.50	0.25	0.50	0.60	3.02	0.40	0.36	0.35	12.6	0.988	---
0.09	0.50	0.25	0.56	0.60	3.60	0.46	0.43	0.22	13.1	0.987	---
0.06	0.50	0.25	0.70	0.60	5.15	0.59	0.58	0.05	17.9	0.975	---
0.16	0.70	0.25	0.30	0.60	1.03	0.20	0.14	0.37	22.7	0.971	---
0.09	0.70	0.25	0.44	0.60	1.91	0.34	0.31	0.45	12.4	0.986	---
0.09	0.70	0.25	0.50	0.60	2.24	0.40	0.38	0.30	11.0	0.9908	---
0.06	0.70	0.25	0.66	0.60	3.20	0.55	0.55	0.03	14.0	0.985	---
0.09	1.00	0.25	0.38	0.60	1.12	0.27	0.25	0.36	15.8	0.988	---
0.09	1.00	0.25	0.43	0.60	1.31	0.33	0.32	0.32	10.0	0.9921	---
0.06	1.00	0.25	0.62	0.60	1.86	0.51	0.51	0.01	11.3	0.9909	---
0.19	0.20	0.25	0.54	0.50	4.61	0.43	0.34	0.32	17.4	0.978	---
0.13	0.20	0.25	0.60	0.50	6.40	0.50	0.44	0.25	21.4	0.966	---
0.10	0.20	0.25	0.65	0.50	8.43	0.56	0.52	0.15	27.0	0.954	---
0.18	0.30	0.25	0.46	0.50	3.05	0.35	0.25	0.41	20.3	0.972	---
0.13	0.30	0.25	0.53	0.50	4.36	0.43	0.36	0.27	18.6	0.976	---
0.10	0.30	0.25	0.59	0.50	5.73	0.49	0.46	0.22	20.6	0.968	---
0.08	0.30	0.25	0.73	0.50	6.88	0.63	0.57	0.20	22.3	0.960	---
0.06	0.30	0.25	0.80	0.50	9.13	0.66	0.66	0.02	27.5	0.937	---
0.18	0.50	0.25	0.34	0.50	1.60	0.23	0.14	0.53	28.7	0.966	---
0.10	0.50	0.25	0.50	0.50	3.02	0.40	0.37	0.34	17.0	0.978	---
0.09	0.50	0.25	0.56	0.50	3.60	0.46	0.43	0.21	16.6	0.980	---
0.06	0.50	0.25	0.70	0.50	5.14	0.59	0.58	0.05	20.4	0.968	---
0.09	0.70	0.25	0.44	0.50	1.91	0.34	0.31	0.42	15.0	0.980	---
0.09	0.70	0.25	0.50	0.50	2.24	0.40	0.38	0.28	14.2	0.985	---
0.09	1.00	0.25	0.38	0.50	1.12	0.27	0.25	0.36	18.4	0.983	---
0.09	1.00	0.25	0.43	0.50	1.31	0.33	0.32	0.32	12.3	0.988	---
0.06	1.00	0.25	0.62	0.50	1.86	0.51	0.51	0.01	13.0	0.988	---
0.58	0.33	0.30	1.00	0.90	0.09	0.17	0.03	-0.25	15.8	0.982	>0.950

Table 1 continued

t_s/d_s	ℓ_g/d_s	t_a/d_s	d_a/d_s	R	$J/V_t^{3/2}$ (nano-pervs/hole)	d_b/d_s	d_{min}/d_s	ℓ_{min}/d_s	α_{max} (deg)	C_f	R_{max}
0.43	0.33	0.30	1.00	0.90	0.27	0.06	0.04	-0.03	19.4	0.977	0.945
0.35	0.33	0.30	1.00	0.90	0.53	0.11	0.06	0.17	20.3	0.977	0.913
0.58	0.33	0.30	1.00	0.80	0.09	0.17	0.03	-0.25	16.8	0.980	---
0.43	0.33	0.30	1.00	0.80	0.27	0.06	0.04	-0.03	21.3	0.973	---
0.35	0.33	0.30	1.00	0.80	0.53	0.11	0.06	0.17	21.6	0.974	---
0.26	0.33	0.30	1.00	0.80	1.04	0.22	0.09	0.49	19.6	0.987	0.840
0.19	0.33	0.30	1.00	0.80	2.00	0.35	0.29	0.55	9.4	0.9980	0.805
0.16	0.33	0.30	1.00	0.80	2.73	0.44	0.36	0.49	6.2	0.9984	0.814
0.12	0.33	0.30	1.00	0.80	3.69	0.52	0.48	0.26	7.7	0.9951	0.810
0.58	0.33	0.30	1.00	0.70	0.09	0.17	0.03	-0.25	18.1	0.977	---
0.43	0.33	0.30	1.00	0.70	0.27	0.06	0.04	-0.03	22.9	0.970	---
0.35	0.33	0.30	1.00	0.70	0.53	0.11	0.06	0.17	23.3	0.969	---
0.26	0.33	0.30	1.00	0.70	1.04	0.22	0.09	0.50	22.5	0.978	---
0.19	0.33	0.30	1.00	0.70	2.00	0.35	0.29	0.54	10.6	0.9955	---
0.16	0.33	0.30	1.00	0.70	2.72	0.44	0.36	0.51	6.8	0.9962	---
0.12	0.33	0.30	1.00	0.70	3.67	0.52	0.48	0.25	10.4	0.9912	---
0.10	0.33	0.30	1.00	0.70	4.95	0.63	0.60	0.15	16.4	0.973	0.779
0.08	0.33	0.30	1.00	0.70	6.63	0.69	0.69	0.05	17.6	0.969	0.773
0.58	0.33	0.30	1.00	0.60	0.09	0.17	0.03	-0.25	19.6	0.972	---
0.43	0.33	0.30	1.00	0.60	0.27	0.06	0.04	-0.03	24.9	0.964	---
0.35	0.33	0.30	1.00	0.60	0.53	0.11	0.06	0.17	25.4	0.964	---
0.26	0.33	0.30	1.00	0.60	1.04	0.22	0.09	0.50	24.6	0.971	---
0.19	0.33	0.30	1.00	0.60	1.99	0.35	0.29	0.52	13.3	0.9898	---
0.16	0.33	0.30	1.00	0.60	2.71	0.44	0.36	0.49	12.2	0.989	---
0.12	0.33	0.30	1.00	0.60	3.66	0.52	0.48	0.24	13.4	0.986	---
0.10	0.33	0.30	1.00	0.60	4.95	0.63	0.60	0.14	19.8	0.960	---
0.08	0.33	0.30	1.00	0.60	6.59	0.69	0.69	0.04	21.2	0.957	---
0.58	0.33	0.30	1.00	0.50	0.09	0.17	0.03	-0.25	21.7	0.967	---
0.43	0.33	0.30	1.00	0.50	0.27	0.06	0.04	-0.03	27.5	0.957	---
0.35	0.33	0.30	1.00	0.50	0.53	0.11	0.06	0.17	28.0	0.957	---
0.26	0.33	0.30	1.00	0.50	1.04	0.22	0.09	0.50	27.1	0.963	---
0.19	0.33	0.30	1.00	0.50	1.99	0.35	0.29	0.51	16.9	0.980	---
0.16	0.33	0.30	1.00	0.50	2.71	0.44	0.37	0.47	15.0	0.983	---
0.12	0.33	0.30	1.00	0.50	3.65	0.52	0.48	0.23	16.9	0.978	---
0.10	0.33	0.30	1.00	0.50	4.91	0.63	0.60	0.14	22.5	0.948	---
0.08	0.33	0.30	1.00	0.50	6.55	0.69	0.69	0.04	24.1	0.944	---
0.58	0.33	0.30	0.44	0.90	0.12	0.18	0.03	-0.26	17.0	0.979	>0.950
0.43	0.33	0.30	0.38	0.90	0.36	0.07	0.04	-0.05	21.8	0.971	>0.950
0.35	0.33	0.30	0.27	0.90	0.73	0.10	0.06	0.14	22.8	0.970	>0.950
0.26	0.33	0.30	0.34	0.90	1.44	0.19	0.08	0.41	19.8	0.988	>0.950
0.19	0.33	0.30	0.43	0.90	2.75	0.33	0.25	0.55	11.3	0.9965	0.938
0.16	0.33	0.30	0.52	0.90	3.70	0.42	0.34	0.52	7.8	0.9988	0.914
0.12	0.33	0.30	0.60	0.90	4.91	0.50	0.45	0.26	5.3	0.9983	0.905
0.58	0.33	0.30	0.44	0.80	0.12	0.18	0.03	-0.26	18.2	0.976	---
0.43	0.33	0.30	0.38	0.80	0.36	0.07	0.04	-0.05	23.3	0.968	---
0.35	0.33	0.30	0.27	0.80	0.73	0.10	0.06	0.13	24.3	0.965	---
0.26	0.33	0.30	0.34	0.80	1.44	0.19	0.08	0.41	23.2	0.979	---
0.19	0.33	0.30	0.43	0.80	2.75	0.33	0.26	0.53	11.3	0.9970	---
0.16	0.33	0.30	0.52	0.80	3.70	0.42	0.34	0.47	7.3	0.9973	---
0.12	0.33	0.30	0.60	0.80	4.91	0.50	0.46	0.25	7.4	0.9953	---
0.10	0.33	0.30	0.73	0.80	6.15	0.60	0.58	0.15	10.2	0.989	0.864
0.08	0.33	0.30	0.83	0.80	7.74	0.68	0.68	0.05	15.0	0.977	0.839
0.12	0.33	0.80	0.60	0.95	4.92	0.50	0.45	0.28	7.3	0.9955	0.952
0.12	0.33	0.50	0.60	0.90	4.91	0.50	0.45	0.28	5.9	0.9969	0.930
0.12	0.33	0.80	0.60	0.90	4.91	0.50	0.45	0.28	7.4	0.9937	---
0.12	0.33	0.30	0.80	0.80	4.35	0.51	0.48	0.23	8.5	0.9940	0.851
0.12	0.33	0.50	0.80	0.80	4.39	0.51	0.47	0.26	10.4	0.9914	0.892
0.12	0.33	0.10	0.60	0.80	4.87	0.50	0.46	0.23	5.9	0.9969	0.840
0.12	0.33	0.50	0.60	0.80	4.91	0.50	0.45	0.28	10.6	0.9935	---
0.12	0.33	0.10	1.00	0.60	3.51	0.52	0.50	0.18	12.0	0.988	0.703
0.12	0.33	0.50	1.00	0.60	3.71	0.52	0.48	0.28	14.8	0.983	---
0.12	0.33	1.00	1.00	0.60	3.73	0.52	0.47	0.32	17.5	0.976	---
0.12	0.33	0.10	0.80	0.60	4.27	0.52	0.49	0.16	13.2	0.986	---
0.12	0.33	0.30	0.80	0.60	4.35	0.51	0.48	0.22	14.7	0.983	---
0.12	0.33	0.50	0.80	0.60	4.35	0.51	0.47	0.26	16.3	0.979	---
0.12	0.33	0.10	0.60	0.60	4.87	0.50	0.47	0.22	12.8	0.987	---
0.12	0.33	0.30	0.60	0.60	4.91	0.50	0.46	0.24	14.9	0.983	---

The maximum value of R, or R_{max}, is the value of R at which the backstreaming of electrons is initiated. There is an effect of ion-beam current, or perveance, on R_{max}. This effect is shown in Fig. 6 for one particular geometry, which was selected because of the wide range of perveance over which solutions had been obtained. R_{max} varies slowly with normalized perveance over most of the range of interest. At small values of perveance, however, R_{max} increases rapidly with decreasing perveance. The R_{max} value at zero perveance corresponds to the Laplace potential solution. Each point in Fig. 6 was obtained from several solutions of the same configuration operated at the same perveance but with different values of R. The saddle point potential in the accelerator hole was determined for each value of R. This saddle point potential changed slightly with R. By extrapolation, an R was found that corresponded to a vanishing barrier for backstreaming electrons.

A backstreaming parameter has been used previously to correlate data for different accelerator-system configurations.[1] This parameter is used in Fig. 7 for about 40 combinations of perveance and accelerator-system geometry. Each point in Fig. 7 represents an extrapolation of the type described previously. The values of R_{max} in Table 1 are also extrapolations of this type, and are therefore shown only for the highest value of R for each combination of perveance and geometry. Some limits were placed on the data included in Fig. 7, however. No data were included in which the perveance was less than 20% of Child's law value (as indicated by normalized perveance) and no extrapolation was used in which the value of $(1-R_{max})$ was less than half of $(1-R)$ for the highest value of R available. The upper limit on the data in Fig. 7 (lowest R_{max} value) is of interest for design purposes. The curve in Fig. 7 represents the equation

$$(1-R_{max})\ell_e/d_a = 0.2\exp(-t_a/d_a)$$

A similar expression with a slightly different constant was proposed earlier.[1] The factor of several increase in data over the previous backstreaming study is believed to justify the change that was made.

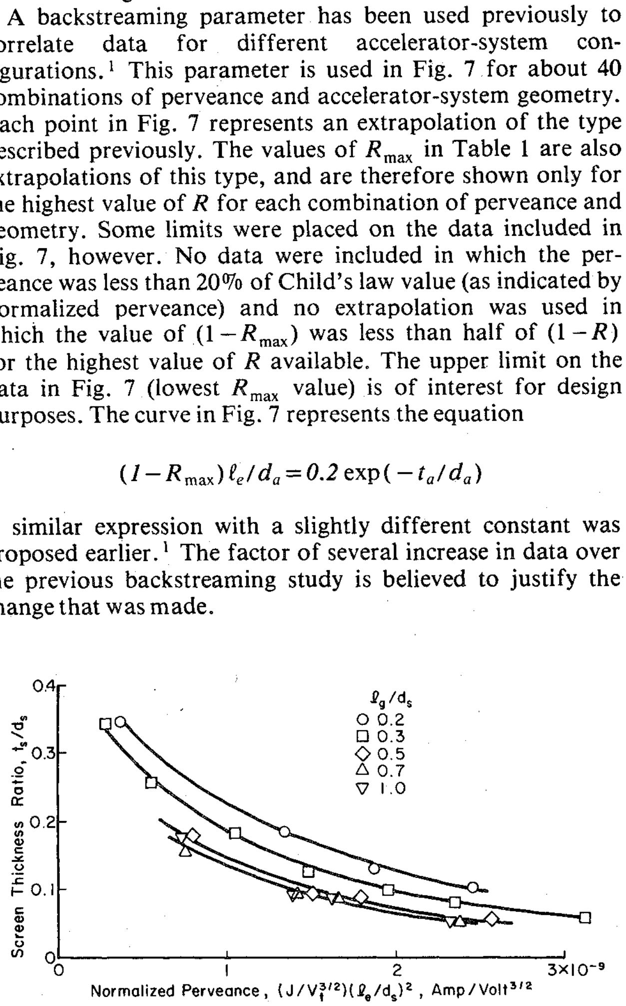

Fig. 5 Screen thickness for all values of R.

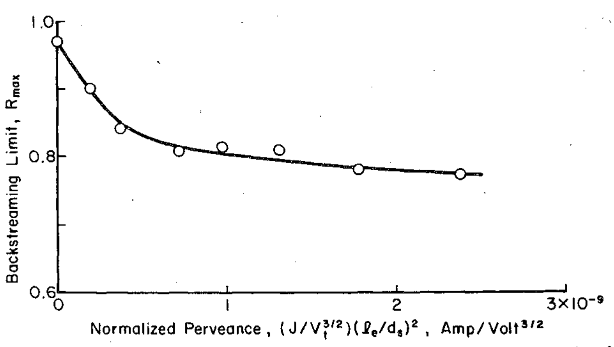

Fig. 6 Variation of backstreaming limit with perveance. $\ell_g/d_s = 0.33$, $d_a/d_s = 1.0$, $t_a/d_s = 0.30$.

Three-Grid Solutions

A 3-grid accelerator system, consisting of screen, accelerator, and decelerator grids was also investigated. Preliminary data indicated that the focusing was insensitive to the hole diameter of the decelerator grid over the range of interest. To be consistent with most solutions calculated for 2-grid systems, the decelerator hole diameter was usually made larger than the largest beam diameter passing through it by 10% of the screen hole diameter. As with the 2-grid survey, however, some solutions were obtained with larger hole diameters. The normalized perveance range was restricted to 1.3 to 2.6×10^{-9} A/V$^{3/2}$ for 3-grid solutions, which was felt to cover most prospective applications.

The beam diameter at the entrance to the accelerator d_b and the screen thickness t_s were all plotted and found to be in close agreement with the plots of the same parameters for 2-grid accelerator systems. Another beam-diameter measurement that is of interest in a 3-grid system is the diameter of the ion beam as it enters the decelerator grid d_b'. This diameter is plotted in Fig. 8. The correlation is excellent below 2×10^{-9} A/V$^{3/2}$, whereas, at higher perveances the spread in beam diameters reaches $\pm0.1\ d_s$. There was also a small consistent trend with R.

The maximum half-angle α_{max} is shown in Fig. 9. This parameter shows reductions over most of the range investigated when compared to the same parameters for 2-grid solutions.

The backstreaming data for 3-grid solutions are few, as indicated by Fig. 10. The same restrictions described for data included in Fig. 7 apply to Fig. 10 while the curve given in Fig. 10 reproduces the curve given in Fig. 7. It is clear from Fig. 10 that the decelerator grid has an adverse effect on R_{max} for small values of ℓ_g/d_s. Such an adverse effect indicates that the decelerator is closer to the accelerator than the closure surface would be in an equivalent 2-grid configuration.

Discussion

As mentioned in the Introduction, the most complete previous study included only 28 solutions.[1] The correlation parameters developed as part of the previous study have, for the most part, been useful in organizing the information obtained in the present study. The most significant difference found in correlation parameters in the two studies was in the parameter used for off-axis beam angles. Not only was the number of solutions quite limited in the previous study, but the solutions were not obtained at parametric values best suited for a correlation of results. For example, the smallest value of ℓ_g/d_s was available at only one value of R, while no single value of t_a/d_s was available at all values of R. The off-axis angle parameters used herein are therefore preferred over those of the previous study.

As a general conclusion, the performance correlations presented herein should be useful in a wide range of multiaperture accelerator-system applications. These

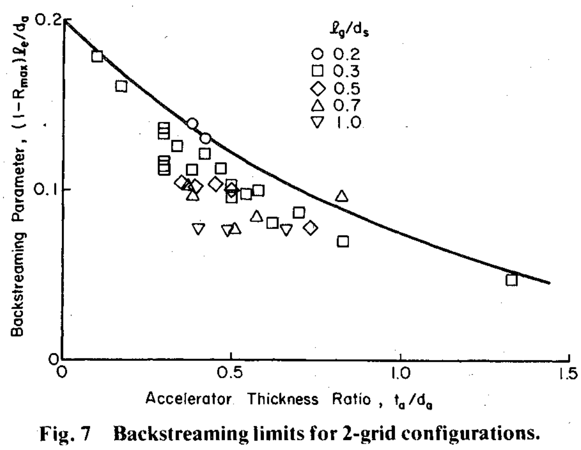

Fig. 7 Backstreaming limits for 2-grid configurations.

Table 2 Three-grid solutions

t_s/d_s	ℓ_g/d_s	t_a/d_s t_d/d_s	d_a/d_s	d_d/d_s	R	$J/V_t^{3/2}$ (nano-pervs/hole)	d_b/d_s	d_b'/d_s	d_{min}/d_s	ℓ_{min}/d_s	α_{max} (deg)	C_f	R_{max}
0.10	0.50	0.25	0.50	0.59	0.90	3.03	0.40	0.38	0.36	0.43	6.3	0.9987	0.936
0.09	0.50	0.25	0.56	0.70	0.90	3.60	0.46	0.47	0.43	0.25	3.9	0.9988	0.924
0.10	0.70	0.25	0.44	0.51	0.90	1.87	0.34	0.31	0.30	0.58	7.1	0.9985	>0.950
0.09	0.70	0.25	0.50	0.62	0.90	2.24	0.40	0.40	0.38	0.34	4.5	0.9993	>0.950
0.06	0.70	0.25	0.67	1.00	0.90	3.20	0.55	0.71	0.55	0.03	7.2	0.9958	0.928
0.09	1.00	0.25	0.37	0.50	0.90	1.12	0.27	0.30	0.25	0.41	8.2	0.9983	>0.950
0.09	1.00	0.25	0.43	0.55	0.90	1.31	0.33	0.38	0.32	0.40	4.9	0.9990	>0.950
0.06	1.00	0.25	0.61	0.88	0.90	1.86	0.51	0.68	0.51	0.01	5.4	0.9978	>0.950
0.19	0.20	0.25	0.54	0.52	0.80	4.62	0.44	0.34	0.34	0.33	9.6	0.9979	0.870
0.10	0.20	0.25	0.66	0.87	0.80	8.38	0.56	0.59	0.52	0.16	10.2	0.9932	0.820
0.13	0.30	0.25	0.53	0.58	0.80	4.37	0.43	0.38	0.36	0.28	9.6	0.9975	0.893
0.10	0.30	0.25	0.59	0.73	0.80	5.74	0.49	0.50	0.46	0.24	6.1	0.9972	0.874
0.08	0.30	0.25	0.73	0.90	0.80	6.90	0.63	0.63	0.56	0.25	9.0	0.9927	0.829
0.10	0.50	0.25	0.50	0.59	0.80	3.03	0.40	0.39	0.36	0.37	6.2	0.9983	---
0.09	0.50	0.25	0.56	0.70	0.80	3.60	0.46	0.48	0.43	0.22	5.4	0.9978	---
0.06	0.50	0.25	0.72	1.06	0.80	5.12	0.59	0.76	0.58	0.05	10.6	0.9903	0.872
0.10	0.70	0.25	0.44	0.51	0.80	1.87	0.34	0.32	0.30	0.51	7.2	0.9983	---
0.09	0.70	0.25	0.50	0.62	0.80	2.24	0.40	0.42	0.38	0.31	5.0	0.9988	---
0.06	0.70	0.25	0.67	1.00	0.80	3.20	0.55	0.74	0.55	0.03	8.5	0.9941	---
0.09	1.00	0.25	0.37	0.50	0.80	1.12	0.27	0.31	0.25	0.35	9.2	0.9974	---
0.09	1.00	0.25	0.43	0.55	0.80	1.31	0.33	0.40	0.32	0.35	5.0	0.9986	---
0.06	1.00	0.25	0.63	0.96	0.80	1.86	0.51	0.71	0.51	0.01	6.8	0.9964	---
0.19	0.20	0.25	0.54	0.52	0.70	4.61	0.44	0.35	0.34	0.29	9.6	0.9976	---
0.10	0.20	0.25	0.66	0.87	0.70	8.36	0.56	0.60	0.52	0.15	12.3	0.9900	---
0.13	0.30	0.25	0.53	0.58	0.70	4.37	0.43	0.39	0.36	0.26	9.6	0.9971	---
0.10	0.30	0.25	0.59	0.73	0.70	5.73	0.49	0.52	0.46	0.22	7.6	0.9959	---
0.08	0.30	0.25	0.73	0.90	0.70	6.90	0.63	0.65	0.57	0.26	10.7	0.9896	---
0.10	0.50	0.25	0.50	0.59	0.70	3.03	0.40	0.40	0.37	0.33	6.2	0.9979	---
0.09	0.50	0.25	0.56	0.70	0.70	3.60	0.46	0.50	0.43	0.21	6.4	0.9970	---
0.06	0.50	0.25	0.72	1.06	0.70	5.11	0.59	0.78	0.59	0.05	12.1	0.988	---
0.10	0.70	0.25	0.44	0.51	0.70	1.87	0.34	0.33	0.30	0.45	7.4	0.9979	---
0.09	0.70	0.25	0.50	0.62	0.70	2.24	0.40	0.43	0.38	0.28	4.5	0.9983	---
0.06	0.70	0.25	0.67	1.00	0.70	3.20	0.55	0.76	0.55	0.03	9.5	0.9926	---
0.09	1.00	0.25	0.37	0.50	0.70	1.12	0.27	0.32	0.25	0.35	10.0	0.9968	---
0.09	1.00	0.25	0.43	0.55	0.70	1.31	0.33	0.41	0.32	0.31	5.2	0.9975	---
0.06	1.00	0.25	0.63	0.96	0.70	1.85	0.51	0.73	0.51	0.01	7.5	0.9959	---
0.19	0.20	0.25	0.54	0.52	0.60	4.61	0.44	0.36	0.34	0.27	9.8	0.9969	---
0.13	0.20	0.25	0.60	0.66	0.60	6.35	0.50	0.48	0.45	0.22	7.8	0.9950	>0.800
0.10	0.20	0.25	0.66	0.87	0.60	8.34	0.56	0.62	0.53	0.14	14.0	0.987	---
0.13	0.30	0.25	0.53	0.58	0.60	4.36	0.43	0.40	0.37	0.24	9.8	0.9964	---
0.10	0.30	0.25	0.59	0.73	0.60	5.72	0.49	0.53	0.46	0.20	8.9	0.9945	---
0.08	0.30	0.25	0.73	0.90	0.60	6.88	0.63	0.66	0.57	0.25	12.1	0.987	---
0.10	0.50	0.25	0.50	0.59	0.60	3.03	0.40	0.37	0.37	0.25	6.4	0.9973	---
0.09	0.50	0.25	0.56	0.70	0.60	3.60	0.46	0.52	0.43	0.20	7.2	0.9961	---
0.06	0.50	0.25	0.72	1.06	0.60	5.11	0.59	0.81	0.59	0.05	13.3	0.985	---
0.10	0.70	0.25	0.44	0.51	0.60	1.87	0.34	0.34	0.31	0.40	7.7	0.9973	---
0.09	0.70	0.25	0.50	0.62	0.60	2.24	0.40	0.45	0.38	0.26	5.3	0.9978	---
0.06	0.70	0.25	0.67	1.00	0.60	3.20	0.55	0.78	0.55	0.03	10.3	0.9912	---
0.09	1.00	0.25	0.37	0.50	0.60	1.12	0.27	0.33	0.25	0.35	10.7	0.9962	---
0.09	1.00	0.25	0.43	0.55	0.60	1.31	0.33	0.42	0.32	0.29	5.4	0.9960	---
0.06	1.00	0.25	0.63	0.96	0.60	1.85	0.51	0.75	0.51	0.01	8.1	0.9951	---
0.19	0.20	0.25	0.54	0.52	0.50	4.60	0.44	0.37	0.35	0.27	10.1	0.9967	---
0.13	0.20	0.25	0.60	0.66	0.50	6.33	0.50	0.49	0.45	0.20	8.5	0.9938	---
0.10	0.20	0.25	0.66	0.87	0.50	8.32	0.56	0.63	0.53	0.13	15.7	0.983	---
0.13	0.30	0.25	0.53	0.58	0.50	4.36	0.43	0.42	0.37	0.23	10.2	0.9956	---
0.10	0.30	0.25	0.59	0.73	0.50	5.72	0.49	0.54	0.47	0.19	9.9	0.9931	---
0.08	0.30	0.25	0.73	0.90	0.50	6.86	0.63	0.68	0.58	0.25	13.7	0.983	---
0.10	0.50	0.25	0.50	0.59	0.50	3.03	0.40	0.43	0.37	0.28	6.6	0.9966	---
0.09	0.50	0.25	0.56	0.70	0.50	3.60	0.46	0.53	0.43	0.19	8.2	0.9951	---
0.06	0.50	0.25	0.72	1.06	0.50	5.10	0.59	0.83	0.59	0.05	14.6	0.982	---
0.10	0.70	0.25	0.44	0.51	0.50	1.87	0.34	0.36	0.31	0.35	8.2	0.9966	---
0.09	0.70	0.25	0.50	0.62	0.50	2.24	0.40	0.46	0.38	0.24	6.1	0.9971	---
0.06	0.70	0.25	0.67	1.00	0.50	3.19	0.55	0.75	0.55	0.03	11.2	0.9898	---
0.09	1.00	0.25	0.37	0.50	0.50	1.12	0.27	0.34	0.25	0.35	11.7	0.9952	---
0.09	1.00	0.25	0.43	0.55	0.50	1.31	0.33	0.44	0.32	0.27	5.9	0.9972	---
0.06	1.00	0.25	0.63	0.96	0.50	1.85	0.51	0.78	0.51	0.00	8.8	0.9944	---
0.13	0.30	0.25	0.60	0.60	0.85	4.25	0.43	0.38	0.37	0.30	9.5	0.9978	0.868
0.10	0.30	0.25	0.60	∞	0.85	5.72	0.49	0.50	0.46	0.25	5.7	0.9975	0.875
0.13	0.30	0.25	0.60	0.60	0.80	4.24	0.43	0.39	0.37	0.28	9.3	0.9976	---
0.13	0.30	0.25	0.60	0.80	0.80	4.24	0.43	0.39	0.37	0.28	9.3	0.9976	0.866

Table 2 continued

t_s/d_s	ℓ_g/d_s	t_a/d_s t_d/d_s	d_a/d_s	d_d/d_s	R	$J/V_t^{3/2}$ (nano-pervs/hole)	d_b/d_s	d_b'/d_s	d_{min}/d_s	ℓ_{min}/d_s	α_{max} (deg)	C_f	R_{max}
0.13	0.30	0.25	0.60	1.00	0.80	4.24	0.43	0.39	0.37	0.29	9.2	0.9975	0.868
0.13	0.30	0.25	0.60	∞	0.80	4.25	0.43	0.39	0.37	0.30	9.0	0.9971	0.869
0.10	0.30	0.25	0.80	0.80	0.80	4.88	0.50	0.53	0.48	0.22	6.6	0.9970	0.804
0.10	0.30	0.25	0.80	1.00	0.80	4.88	0.50	0.53	0.48	0.22	6.7	0.9969	0.805
0.10	0.30	0.25	0.80	∞	0.80	4.89	0.50	0.53	0.48	0.23	8.5	0.9953	0.816
0.10	0.30	0.25	0.60	0.80	0.80	5.71	0.49	0.51	0.46	0.22	6.5	0.9970	0.870
0.10	0.30	0.25	0.60	1.00	0.80	5.71	0.49	0.51	0.46	0.22	6.7	0.9968	0.871
0.10	0.30	0.25	0.60	∞	0.80	5.72	0.49	0.50	0.46	0.25	8.2	0.9955	---
0.08	0.30	0.25	0.80	1.00	0.80	6.58	0.63	0.64	0.57	0.26	9.0	0.9925	0.809
0.13	0.30	0.25	0.80	∞	0.80	6.59	0.63	0.63	0.57	0.26	10.0	0.9909	0.818
0.13	0.30	0.25	1.00	1.00	0.70	2.89	0.44	0.39	0.39	0.40	8.3	0.9977	0.722
0.13	0.30	0.25	1.00	∞	0.70	2.92	0.44	0.38	0.38	0.43	8.0	0.9962	0.764
0.13	0.30	0.25	0.80	0.80	0.70	3.65	0.42	0.40	0.38	0.28	8.4	0.9976	0.780
0.13	0.30	0.25	0.60	0.60	0.70	4.24	0.43	0.40	0.37	0.26	9.2	0.9972	---
0.13	0.30	0.25	0.60	0.80	0.70	4.24	0.43	0.40	0.37	0.26	9.1	0.9969	---
0.13	0.30	0.25	0.60	1.00	0.70	4.24	0.43	0.40	0.37	0.27	9.1	0.9968	---
0.13	0.30	0.25	0.60	∞	0.70	4.24	0.43	0.39	0.37	0.29	9.4	0.9938	---
0.10	0.30	0.25	0.80	0.80	0.70	4.86	0.51	0.55	0.48	0.20	8.5	0.9952	---
0.10	0.30	0.25	0.80	1.00	0.70	4.86	0.50	0.55	0.48	0.20	8.9	0.9948	---
0.10	0.30	0.25	0.80	∞	0.70	4.88	0.50	0.52	0.48	0.22	12.5	0.9899	---
0.08	0.30	0.25	1.00	1.00	0.70	5.24	0.64	0.65	0.58	0.25	10.1	0.9910	0.716
0.08	0.30	0.25	1.00	∞	0.70	5.30	0.64	0.64	0.58	0.25	13.1	0.986	0.755
0.10	0.30	0.25	0.60	0.80	0.70	5.71	0.49	0.52	0.47	0.20	8.0	0.9956	---
0.10	0.30	0.25	0.60	1.00	0.70	5.71	0.49	0.52	0.47	0.20	8.7	0.9949	---
0.10	0.30	0.25	0.60	∞	0.70	5.71	0.49	0.51	0.46	0.22	12.7	0.989	---
0.08	0.30	0.25	0.80	1.00	0.70	6.57	0.64	0.65	0.58	0.26	10.9	0.989	---
0.08	0.30	0.25	0.80	∞	0.70	6.59	0.64	0.64	0.57	0.26	14.0	0.983	---
0.13	0.30	0.25	1.00	1.00	0.60	2.85	0.45	0.41	0.40	0.34	8.0	0.9968	---
0.13	0.30	0.25	1.00	∞	0.60	2.91	0.44	0.39	0.41	0.38	9.9	0.9927	---
0.13	0.30	0.25	0.80	0.80	0.60	3.63	0.43	0.41	0.38	0.25	8.2	0.9966	---
0.13	0.30	0.25	0.80	∞	0.60	3.66	0.42	0.39	0.38	0.29	11.7	0.9903	>0.800
0.13	0.30	0.25	0.60	0.60	0.60	4.23	0.43	0.41	0.38	0.23	9.4	0.9965	---
0.13	0.30	0.25	0.60	0.80	0.60	4.23	0.43	0.41	0.37	0.24	9.2	0.9958	---
0.13	0.30	0.25	0.60	1.00	0.60	4.23	0.43	0.41	0.37	0.24	9.1	0.9955	---
0.13	0.30	0.25	0.60	∞	0.60	4.24	0.43	0.39	0.37	0.27	13.3	0.988	---
0.10	0.30	0.25	0.80	0.80	0.60	4.83	0.51	0.57	0.49	0.18	9.9	0.9934	---
0.10	0.30	0.25	0.80	1.00	0.60	4.84	0.51	0.56	0.49	0.18	10.7	0.9924	---
0.10	0.30	0.25	0.80	∞	0.60	4.87	0.50	0.54	0.48	0.21	15.9	0.984	---
0.08	0.30	0.25	1.00	1.00	0.60	5.18	0.65	0.68	0.59	0.25	12.1	0.987	---
0.08	0.30	0.25	1.00	∞	0.60	5.27	0.64	0.65	0.58	0.25	16.7	0.977	---
0.10	0.30	0.25	0.60	0.80	0.60	5.70	0.49	0.55	0.47	0.19	9.4	0.9939	---
0.10	0.30	0.25	0.60	1.00	0.60	5.70	0.49	0.52	0.47	0.19	10.2	0.9928	---
0.10	0.30	0.25	0.60	∞	0.60	5.71	0.49	0.51	0.47	0.21	16.3	0.980	---
0.08	0.30	0.25	0.80	1.00	0.60	6.54	0.64	0.67	0.58	0.26	12.6	0.985	---
0.08	0.30	0.25	0.80	∞	0.60	6.58	0.64	0.65	0.57	0.26	17.9	0.973	---
0.13	0.30	0.25	1.00	1.00	0.50	2.82	0.45	0.43	0.41	0.30	7.9	0.9952	---
0.13	0.30	0.25	1.00	∞	0.50	2.90	0.44	0.39	0.39	0.40	13.0	0.987	---
0.13	0.30	0.25	0.80	0.80	0.50	3.61	0.43	0.43	0.39	0.21	8.5	0.9952	---
0.13	0.30	0.25	0.80	1.00	0.50	3.62	0.43	0.43	0.39	0.22	8.2	0.9949	>0.750
0.13	0.30	0.25	0.80	∞	0.50	3.66	0.42	0.40	0.38	0.28	15.5	0.983	---
0.13	0.30	0.25	0.60	0.60	0.50	4.23	0.43	0.42	0.38	0.22	9.7	0.9956	---
0.13	0.30	0.25	0.60	0.80	0.50	4.23	0.43	0.42	0.38	0.22	9.6	0.9941	---
0.13	0.30	0.25	0.60	1.00	0.50	4.23	0.43	0.42	0.38	0.23	9.7	0.9934	---
0.13	0.30	0.25	0.60	∞	0.50	4.24	0.43	0.40	0.37	0.27	17.5	0.979	---
0.10	0.30	0.25	0.80	0.80	0.50	4.81	0.51	0.59	0.49	0.16	11.5	0.9911	---
0.10	0.30	0.25	0.80	1.00	0.50	4.82	0.51	0.58	0.49	0.17	12.6	0.989	---
0.10	0.30	0.25	0.80	∞	0.50	4.87	0.51	0.55	0.48	0.20	19.4	0.975	---
0.08	0.30	0.25	1.00	1.00	0.50	5.12	0.65	0.70	0.60	0.25	14.1	0.982	---
0.08	0.30	0.25	1.00	∞	0.50	5.25	0.62	0.66	0.58	0.25	20.3	0.967	---
0.10	0.30	0.25	0.60	0.80	0.50	5.69	0.49	0.55	0.47	0.18	10.7	0.9921	---
0.10	0.30	0.25	0.60	1.00	0.50	5.70	0.49	0.54	0.47	0.18	12.0	0.9902	---
0.10	0.30	0.25	0.60	∞	0.50	5.71	0.49	0.52	0.47	0.21	20.2	0.972	---
0.08	0.30	0.25	0.80	1.00	0.50	6.51	0.64	0.69	0.58	0.24	14.3	0.981	---
0.08	0.30	0.25	0.80	∞	0.50	6.57	0.64	0.66	0.58	0.26	21.7	0.961	---

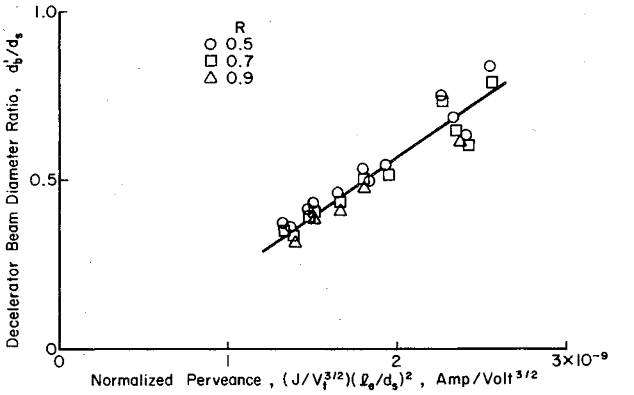

Fig. 8 Ion-beam diameter at entrance to decelerator hole. $\ell_g/d_s = 0.2\text{-}0.7$.

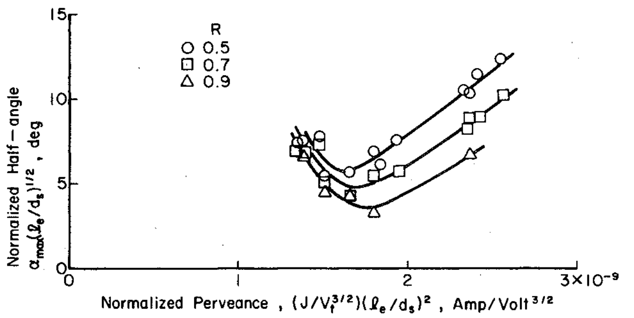

Fig. 9 Normalized beam spread for 3-grid configurations. $\ell_g/d_s = 0.2\text{-}0.7$.

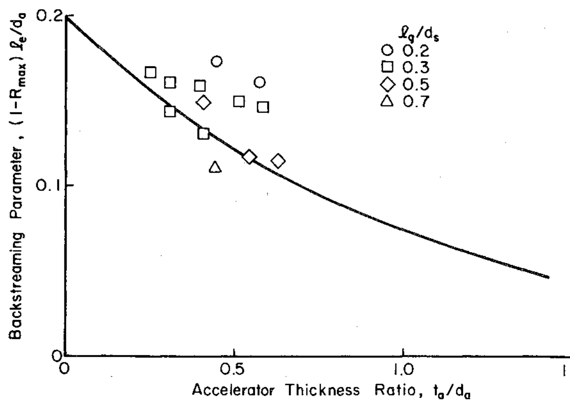

Fig. 10 Backstreaming limits for 3-grid configurations.

correlations appear accurate within the data scatter for R values from 0.5 to 0.9 and interelectrode gap ratios ℓ_g/d_s of 0.2 to 0.5. The correlations are still fair at an ℓ_g/d_s of 0.7. Additional solutions, beyond those included in the correlations, are presented in the tables.

The screen thicknesses obtained for the accelerator-system solutions represent a restriction on the use of these solutions. There is, for each electrode configuration, a single family of plasma-sheath shapes that cover the range of perveance investigated. This means that the selection of an electrode configuration and perveance uniquely defines the interception of the plasma sheath with the screen-hole radius. These interceptions have been used for the screen thicknesses presented in Fig. 5. It is possible to obtain experimental operation where the screen is thinner than the value obtained from Fig. 5. Such operation involves a detached plasma sheath, with some ions being extracted from a radius larger than the screen hole radius. Experimentally, it is also possible to operate with a thicker screen than given by Fig. 5, but the computer simulation of such a configuration is not possible at the present time. Such a thick screen would extend back into the plasma, resulting in the additional recombination of ions on the screen surface. As a result of this recombination, the plasma density would be greatest at the center of a screen hole and fall off toward the outside of the hole (at the screen hole radius). Although present computer programs can be iterated for a nonuniform current density just as easily as a uniform one, the degree of nonuniformity that a thick screen would cause cannot be predicted at the present time. The solutions presented herein are also limited by the plasma sheath being at screen potential. This means that the solutions are most applicable when the discharge voltage is negligible compared to the total accelerating voltage.

A number of conclusions of interest for accelerator-system design can be drawn from the solutions presented herein. One such conclusion concerns trajectory crossover. A rise in the accelerator impingement ratio (fraction of ion-beam current) is often found at low ion-beam currents. This rise has been attributed to the plasma sheath receding and becoming more concave, so that ions from the outside edge of a hole cross over during acceleration and strike the edge of the accelerator hole on the opposite side. Crossover, as just described, was not encountered in any solutions for geometries that are consistent with current practice. Those experimental configurations in which an impingement ratio rise is found at low beam currents usually involve a contributing factor, the most common of which is a large variation in plasma density across the screen hole. This variation results in a skewed plasma sheath that directs the beam through that screen aperture toward the low-density side of the accelerator hole. The observable result of this effect is small notches on the outside edges of the outer holes in multiaperture accelerator systems.

A small angular divergence and a large beam current are desired for most ion-beam applications. As a result, the usual range of interest for normalized perveance is from about 1.5 to 3.0×10^{-9}. For this range, the smallest 2-grid beam divergence is obtained with the smallest accelerator hole diameter and smallest accelerator thickness. Unless operation is required over a wide range of perveance, the small accelerator hole will usually pose no problem, inasmuch as it also tends to reduce the loss of un-ionized propellant, increase the potential barrier to prevent electron back-streaming, and increase the amount of material available to withstand charge-exchange erosion. The selection of accelerator thickness is not so straightforward, inasmuch as a tradeoff study may be required. Reduction of the accelerator thickness improves ion-beam focusing, but it also increases the loss of un-ionized propellant, decreases the potential barrier for backstreaming, and decreases the material available for wear. For many ion thruster applications, however, it appears that the saving in propellant that could be obtained with a thicker accelerator would more than offset the decrease in thrust coefficient.

Again considering the normalized perveance range from 1.5 to 3.0×10^{-9}, comparison of Figs. 4 and 9 shows that the addition of a decelerator grid usually decreases beam divergence. This advantage of a decelerator grid becomes negligible as R approaches R_{max}.

Concluding Remarks

Space-charge-flow solutions are presented in both tabular form and generalized graphic form for a wide range of geometries and operating conditions. The generalized graphic approach is particularly useful for presenting a wide range of solutions in a compact format. Some specific conclusions can be drawn from the solutions.

1) Trajectory crossover is unlikely to be the cause of high impingement ratios in 2-grid configurations at low ion-beam currents.

2) The focusing of 2-grid configurations is generally improved as the deceleration voltage, the accelerator thickness, and the accelerator hole diameter are decreased.

3) Use of a grounded decelerator usually improves focusing over the equivalent 2-grid configuration. This improvement becomes negligible as the net-to-total voltage ratio approaches the backstreaming limit.

Acknowledgment

This work was performed under NASA Grant NGR-06-002-112.

References

[1]Kaufman, H.R., *Advances in Electronics and Electron Physics,*" Vol. 36 (L. Marton, ed.). Academic Press, New York, 1974, pp. 265-373.

[2]Lathem, W.C., "Ion Accelerator Designs for Kaufman Thrusters," *Journal of Spacecraft and Rockets,* Vol. 6, Nov. 1969, pp. 1237-1242.

[3]Lathem, W.C., personal communication, 1973.

[4]Nudd, G.R., Amboss, K., "Effects of Electrode Misalignment and Flow Rate Changes on the Thrust in an Electron-Bombardment Engine," *AIAA Journal,* Vol. 8, April 1970, pp. 649-656.

[5]Bogart, C.D. and Richley, E.A., NASA TN D-3394, 1966.

[6]Hyman, J., Jr., Echkhardt, W.O., Knechtli, R.C., and Buckey, C.R., *AIAA Journal,* Vol. 2, Oct. 1964, pp. 1739-1748.

[7]Pawlik, E.V., Margosian, P.M., and Staggs, J.F., "A Technique for Obtaining Plasma-Sheath Configurations and Ion Optics for an Electron-Bombardment Thruster," NASA TN D-2804, May 1965.